Scattering matrix invariants of Floquet topological insulators

I. C. Fulga and M. Maksymenko[*]

Department of Condensed Matter Physics, Weizmann Institute of Science, Rehovot 76100, Israel

Similar to static systems, periodically driven systems can host a variety of topologically nontrivial phases. Unlike the case of static Hamiltonians, the topological indices of bulk Floquet bands may fail to describe the presence and robustness of edge states, prompting the search for new invariants. We develop a unified description of topological phases and their invariants in driven systems by using scattering theory. We show that scattering matrix invariants correctly describe the topological phase, even when all bulk Floquet bands are trivial. Additionally, we use scattering theory to introduce and analyze new periodically driven phases, such as *weak topological Floquet insulators*, for which invariants were previously unknown. We highlight some of their similarities with static systems, including robustness to disorder, as well as some of the features unique to driven systems, showing that the weak phase may be destroyed by breaking translational symmetry not in space, but in time.

I. INTRODUCTION

Topologically nontrivial phases are characterized by the simultaneous presence of an insulating bulk and robust, conducting edge states [1,2]. The boundaries are protected against localization by the system's bulk properties, namely its symmetries and the presence of a mobility gap. This link is termed bulk-boundary correspondence, and it enables us to define topological invariants, $\mathbb{Z}$- or $\mathbb{Z}_2$-valued quantities computed from the bulk system, which determine the presence and number of protected gapless modes at the boundary.

The number and nature of topological invariants have been studied extensively for static Hamiltonians. For noninteracting systems, there exist classifications of symmetry-protected topological insulators and superconductors [3–11]. Their boundary states can be protected not only by the three fundamental symmetries of the system—i.e., time-reversal, particle-hole, and chiral symmetry—but also by the symmetries of the underlying lattice. The latter are known as weak topological insulators in the case of translation symmetry or topological crystalline insulators for point-group symmetries (reflection, rotation, etc.), and they can exist in both two and three space dimensions [12–18]. Recent experiments have shown evidence for the existence and robustness of both [19–22].

Beyond static Hamiltonians, the topological phases of periodically driven systems have recently become the focus of a wide range of research [23–25]. Part of the appeal of so-called Floquet topological insulators is the possibility to change a system's properties by altering the driving field [26,27]. While the physical properties of time-independent systems are mostly fixed during the fabrication process, a Floquet system can in principle host a variety of topological phases as a function of an external, time-periodic perturbation. Examples include phases hosting Floquet Majorana fermions [28–31], as well as robust chiral [32–36], helical [26,37], or counterpropagating edge modes [38–42]. Possible extensions of these ideas to interacting systems have also been actively discussed [43,44].

In spite of this intense activity, the topological nature of periodically driven systems is much less understood as

compared to their time-independent counterparts. Unlike wave functions of static systems, Floquet states are obtained from the unitary time-evolution operator over one driving period, the so-called Floquet operator, $\mathcal{F}$. Each of its eigenstates accumulates a phase factor during one period T of the time evolution, as $\mathcal{F}|\psi\rangle = \exp(-i\varepsilon T/\hbar)|\psi\rangle$, with ε referred to as quasienergy. While the Floquet states and their associated quasienergies are in many ways analogous to the eigenstates and energies of static systems, the periodic nature of the driving means that ε is only defined modulo $2\pi\hbar/T$. The periodicity of the resulting Brillouin zone (BZ) in quasienergy can lead to situations in which the original topological invariants fail to correctly capture the system's behavior at an edge. Indeed, in Ref. [33] it was shown that robust chiral edge states can form in a system in which all bulk bands are trivial, since the Floquet operator in the bulk equals the unit matrix, $\mathcal{F} = \mathbb{1}$.

Several works have made progress toward a full classification of Floquet topological insulators [45,46]. In some cases, novel invariants have been formulated, which take into account the system's driven nature. For strong two-dimensional (2D) Floquet topological insulators, invariants have been found, both in the presence and absence of time-reversal symmetry [33,37]. Weak topological effects, however, have remained largely unexplored. Among the few examples to date, 2D chiral-symmetric systems hosting anomalous counterpropagating edge modes have been reported in Refs. [38–40,42]. In these works, the existence and robustness to disorder of edge modes was identified, but the topological index responsible for their presence has remained unknown up to now.

To accurately predict the possible nontrivial phases, the properties of Floquet topological insulators—both weak and strong—need to be treated within a unified framework. Toward that end, rather than focusing on their difference with respect to static systems, we take advantage of their similarities instead. In both types of phases, topological properties manifest themselves at the (quasi-)Fermi-level, in the form of robust conducting edge modes, which exhibit similar forms of spectral flow. As such, their nontrivial phases can be characterized in a unified manner by using scattering theory.

Previous works have considered the quantum transport properties of Floquet systems [47–50]. The scattering problem is typically defined in terms of a driven sample connected to

---

[*]On leave from the Institute for Condensed Matter Physics, National Academy of Sciences of Ukraine, L'viv-79011, Ukraine.

multiple metallic electrodes, and the scattering matrix relates the amplitudes of asymptotic scattering states in the metallic leads. In contrast, our main focus is not studying transport properties but establishing a topological classification of Floquet systems in terms of the scattering matrix. Toward that end, rather than attaching metallic electrodes, we impose absorbing boundary conditions on a given sample to define a simplified, yet fictitious, scattering problem [51]. As we will show, the resulting scattering matrix enables us to fully determine the topological properties of periodically driven systems.

The Fermi level scattering matrix has been used to formulate both strong and weak topological invariants for time-independent Hamiltonians [52,53] as well as 1D quantum walks [54], having the advantage of being naturally tailored to the study of disordered systems. In this work, we extend this approach to periodically driven systems, showing different examples of its application. Specifically, we formulate topological invariants for the models of Refs. [38,42], based on the constraints imposed on the scattering matrix by the symmetries of the system. Furthermore, we show that the original scattering matrix invariants developed to characterize strong and weak *static* topological insulators can be readily applied to driven systems, even in cases in which all bulk Floquet bands are trivial. This unified approach mitigates the need for new topological indices, enabling the study of a wide class of both static and driven phases using the same invariant expressions. As an example, we turn to the model studied in Ref. [45] and reveal a richer topological structure consisting of both strong and weak phases. We showcase some features of weak phases that are unique to periodically driven systems, such as the possibility of gapping out the edge modes by breaking translation symmetry in time.

The rest of our work is organized as follows. In Sec. II, we study the chiral-symmetric Floquet system of Refs. [38,42]. We determine the scattering matrix invariant and, based on its structure, predict the localization behavior of edge states in the presence of disorder. We find nontrivial phases of a $\mathbb{Z}_2$ (as opposed to $\mathbb{Z}$) nature, and we conclude that the edge states are not robust to disorder that does not preserve chiral symmetry, contrary to previous reports. We confirm this expectation by performing numerical simulations. In Sec. III, we turn to the particle-hole symmetric Floquet topological insulator of Ref. [45], which hosts both strong and weak topological phases. We find that the original, strong, and weak scattering matrix invariants accurately describe the edge-state robustness, even though all bulk bands are trivial. We conclude in Sec. IV.

II. CHIRAL SYMMETRIC DRIVEN SYSTEM

To date, there have been few studies on weak topological effects in periodically driven systems. References [38,42] have observed this behavior in 2D systems possessing chiral symmetry. In this section, we turn to one such model, the *kicked quantum Hall* system, and we use scattering theory to determine its topological invariant.

The model describes spinless fermions on a square lattice (lattice constant $a = 1$), where the position of each site is given by the vector $\mathbf{r} = n_x \hat{x} + n_y \hat{y}$, with $n_{x,y}$ integers and $\hat{x}, \hat{y}$ unit vectors pointing in the x and y directions, respectively.

The tight-binding Hamiltonian

$$H_{\text{KQH}} = \frac{J_x}{2} \sum_{n_x, n_y} |n_x + 1, n_y\rangle\langle n_x, n_y|$$
$$+ \frac{J_y}{2} e^{in_x\alpha} |n_x, n_y + 1\rangle\langle n_x, n_y| + \text{H.c.} \quad (1)$$

is expressed in terms of states $|n_x, n_y\rangle$ on lattice sites indexed by (n_x, n_y). Here, $J_{x,y}$ are the nearest-neighbor hopping amplitudes in the x and y directions. The system is placed in a uniform magnetic field, with α modeling the flux threaded in each plaquette.

In the static case, Eq. (1) is the well-studied Hofstadter model [55], showing a fractal pattern of gapped, Chern-insulating phases. As in Refs. [38,42], we take $J_{x,y}$ to be periodic functions of time, with $J_x(t) = J_x$ and $J_y(t) = J_y \sum_m \delta(t - m), m \in \mathbb{Z}$. In other words, the hopping in the x direction is kept constant, while the coupling in the y direction is turned on periodically with a period $T = 1$, but only at discrete times $t = m$.

When the system is infinite in one or more directions, or alternatively in the presence of periodic boundary conditions (PBCs), momentum becomes a good quantum number, enabling us to express Eq. (1) in reciprocal space. The time-dependent momentum-space Hamiltonian becomes

$$\mathcal{H}_{\text{KQH}} = J_x \cos(k_x) + J_y \cos(k_y - n_x\alpha) \sum_m \delta(t - m), \quad (2)$$

where n_x labels sites in the magnetic unit cell.

As long as there are no on-site potentials, the model shows chiral symmetry, expressed as a staggered gauge transformation. The chiral symmetry operator changes the sign of the wave function on one of the two sublattices,

$$\Gamma : |n_x, n_y\rangle \rightarrow (-1)^{n_x + n_y} |n_x, n_y\rangle. \quad (3)$$

It is a unitary operator, $\Gamma^\dagger \Gamma = \Gamma^2 = 1$. In real space it anticommutes with the Hamiltonian, $\Gamma H_{\text{KQH}} \Gamma = -H_{\text{KQH}}$, while in reciprocal space it amounts to a π shift in momentum,

$$\Gamma \mathcal{H}_{\text{KQH}}(k_x, k_y) \Gamma = \mathcal{H}_{\text{KQH}}(k_x + \pi, k_y + \pi)$$
$$= -\mathcal{H}_{\text{KQH}}(k_x, k_y). \quad (4)$$

We set $\hbar = 1$ and define the Floquet operator as propagating states from $t = 0.5$ to 1.5:

$$\mathcal{F}_{\text{KQH}} = \exp\left(-i \int_{0.5}^{1.5} \mathcal{H}_{\text{KQH}}(t) \, dt\right). \quad (5)$$

In this so-called symmetric time frame [56,57], Eq. (5) can be written as

$$\mathcal{F}_{\text{KQH}} = e^{-i\frac{J_x}{2}\cos(k_x)} e^{-iJ_y\cos(k_y - n_x\alpha)} e^{-i\frac{J_x}{2}\cos(k_x)}. \quad (6)$$

Due to the chiral symmetry of the periodically modulated Hamiltonian (2), the Floquet operator (6) also shows chiral symmetry, expressed as

$$\Gamma_{\mathcal{F}} = \exp(in_x\pi) \exp(in_y\pi). \quad (7)$$

While on the Hamiltonian level chiral symmetry amounts to changing the sign of the eigenvalues, in Floquet language it reverses the direction of the time evolution,

$$\Gamma_{\mathcal{F}} \mathcal{F}_{\text{KQH}} \Gamma_{\mathcal{F}} = \mathcal{F}_{\text{KQH}}^\dagger. \quad (8)$$
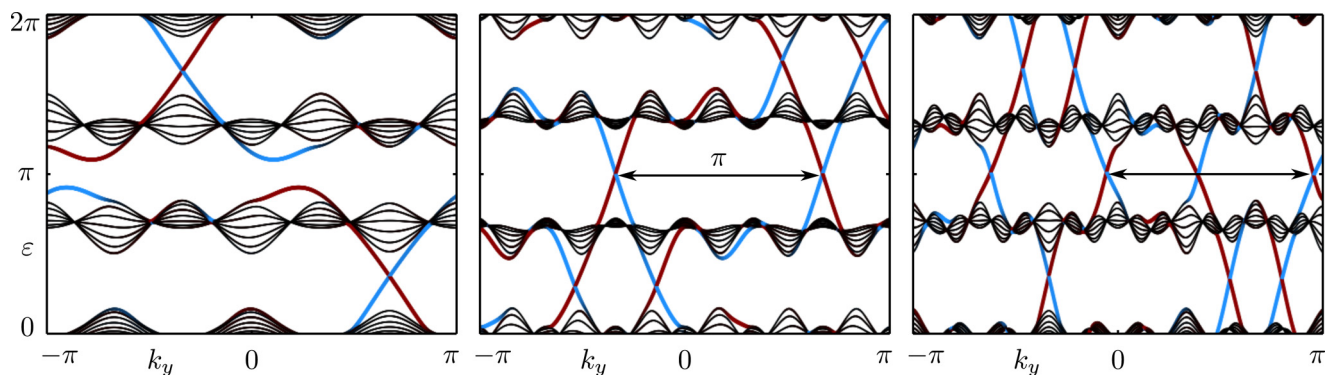
FIG. 1. Band structure of the Floquet operator (6) in an infinite strip geometry (infinite in y, $L = 21$ sites in the x direction). Parameters are $\alpha = 2\pi/3$, $J_x = 2\pi/3$, and $J_y = \pi, 2\pi, 3\pi$ in the left, middle, and right panels, respectively. Red (dark gray) indicates states localized on the left boundary and blue (light gray) indicates states on the right. From left to right, the bulk gap at $\varepsilon = \pi$ shows zero, one, or two pairs of counterpropagating edge modes, separated by a momentum difference $\Delta k_y = \pi$ (horizontal arrows).

We set $\alpha = 2\pi/3$, such that the system has three bulk Floquet bands. In the following, we consider Eq. (6) either in a strip geometry (infinite in y, finite in x) or discretized on a square lattice of $L \times W$ sites. All numerical results are obtained for tight-binding models defined using the KWANT code [58,59].

Typical band structures obtained by diagonalizing the Floquet operator $\mathcal{F}_{\mathrm{KQH}}|\psi\rangle = \exp(-i\varepsilon)|\psi\rangle$ in an infinite strip geometry are shown in Fig. 1. As a function of the parameters $J_{x,y}$, the model exhibits a variety of topological phases. The top and bottom quasienergy gaps of Fig. 1 ($\varepsilon = \pi/2$ and $\varepsilon = 3\pi/2$) show one or more edge modes with a nonzero net chirality, a feature reminiscent of the quantum Hall effect. The boundary modes occur on all edges, irrespective of orientation, and they have been understood [42] in terms of the Floquet winding number of Ref. [33].

We focus on edge modes in the gap at $\varepsilon = \pi$, which have no net chirality but come in counterpropagating pairs. Each pair is separated by a momentum difference of π. Furthermore, unlike boundary states in the top and bottom gaps, the counterpropagating modes depend on the orientation of the edge, similar to weak topological insulators. For the values of $J_{x,y}$ used in the left panel of Fig. 1, there are no gapless edge states on boundaries parallel to either the x or y direction. In the middle panel both types of boundary show one pair of edge modes, while in the right panel there are two pairs on the edge parallel to y, and none along x. There is to date no known topological invariant responsible for the presence and robustness of these edge states.

The presence of counterpropagating modes has been previously identified as being a consequence of chiral symmetry. Indeed, in a strip geometry the relation (8) becomes

$$\Gamma_{\mathcal{F}} \mathcal{F}_{\mathrm{KQH}}(k_y) \Gamma_{\mathcal{F}} = \mathcal{F}_{\mathrm{KQH}}^{\dagger}(k_y - \pi), \qquad (9)$$

such that for each state at energy ε and momentum k_y there must be a state at $-\varepsilon$ and $k_y - \pi$. Therefore, edge modes at $\varepsilon = \pm\pi$ necessarily come in pairs. In the following, we will determine the nature of this topological phase as well as the explicit form of its topological invariant.

In the absence of disorder, momentum is a good quantum number and a single pair of edge states is protected, since the states must be separated by a momentum difference $\Delta k_y = \pi$.

Figure 1 also shows a situation in which there are two pairs of counterpropagating modes at $\varepsilon = \pi$, raising the question of whether this is a distinct phase or whether different pairs of edge modes can annihilate and gap out if they overlap. The answer will determine whether the phase is of a $\mathbb{Z}$ type, with any number of protected edge modes, or of a $\mathbb{Z}_2$ type, where only an odd number of pairs is protected. We test this hypothesis in a controllable fashion by considering two copies of Eq. (1), coupled in such a way as to preserve the chiral symmetry (3) of the combined system (see Fig. 2). Each of the two subsystems has one pair of edge modes, but one of them is shifted in momentum relative to the other, $k_y \to k_y + \delta$. This enables us to effectively *slide* one pair of edges in the quasi-BZ by changing the value of δ. In a strip geometry, the Hamiltonian of the combined system has the form

$$
\begin{aligned}
H_{2\times\mathrm{KQH}} = \sum_{n_x} \Bigg(&\frac{J_x}{2} \sum_{j=1,2} |n_x, j + 1\rangle\langle n_x, j| \\
&+ \frac{J_y}{2} e^{in_x\alpha + ik_y} |n_x, 1\rangle\langle n_x, 1| \\
&+ \frac{J_y}{2} e^{in_x\alpha + i(k_y+\delta)} |n_x, 2\rangle\langle n_x, 2| \\
&+ \frac{J_c}{2} \sum_{j\neq j'} e^{ik_y} |n_x, j\rangle\langle n_x, j'| + \mathrm{H.c.} \Bigg),
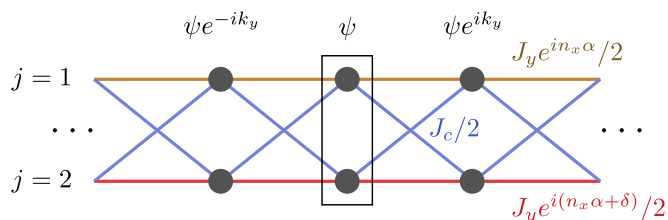\end{aligned} \qquad (10)
$$

FIG. 2. Side view of the Hamiltonian (10), consisting of two copies of (1) labeled by $j = 1,2$ (top and bottom layers). One of the three unit cells shown is marked by a box. The coupling within the top and bottom layers is marked with orange and red lines, respectively, while that between the layers is shown in blue. Notice that chiral symmetry is preserved, as there is no coupling between layers in the same unit cell.
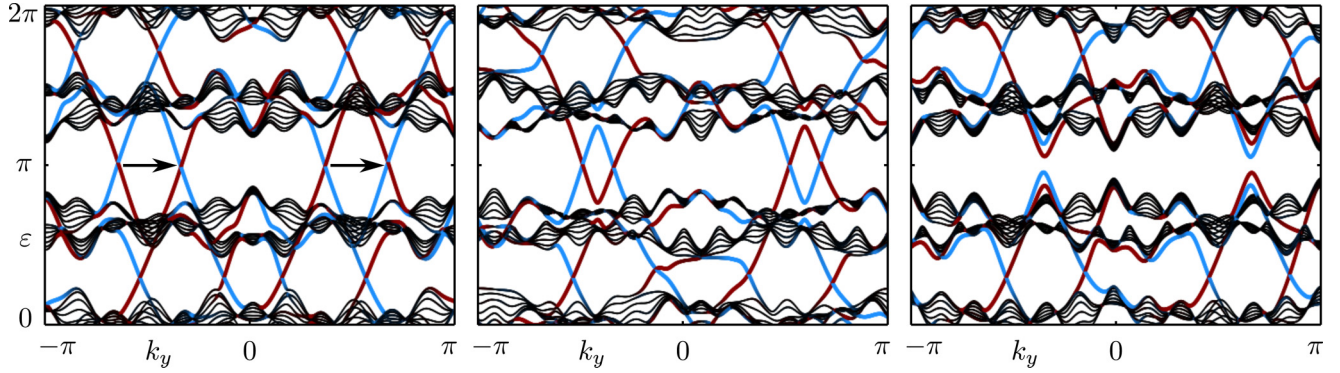
FIG. 3. Band structures of the model (10) in the same geometry as Fig. 1. We set $\alpha = J_x = 2\pi/3$, $J_y = 2\pi$, and $J_c = 0.6$. In the left, middle, and right panels, $\delta = 0.7\pi$, 0.85π, and 0.98π, respectively. Sliding one pair of edge modes on top of the other (horizontal arrows) causes them to annihilate and opens gaps in the spectrum. This indicates they are protected by a $\mathbb{Z}_2$ invariant.

where the index $j^{(\prime)} = 1,2$ labels the two copies, and J_c is the time-independent coupling between them. In Fig. 3, we show that as the two pairs of edge modes are made to overlap, gaps open in the spectrum. Therefore, there are only two topologically distinct edge mode configurations, one pair of counterpropagating modes versus no edge modes, indicating that the nontrivial phase is protected by a $\mathbb{Z}_2$ as opposed to a $\mathbb{Z}$ invariant.

To construct this invariant as well as test the conducting properties of the edge, we turn to the scattering matrix formalism. For a static Hamiltonian discretized on a finite lattice, transport properties are usually obtained by connecting one or more infinite, translationally invariant leads to the system. This enables us to compute the scattering matrix, which in the two-lead case reads

$$S = \begin{pmatrix} r & t \\ t' & r' \end{pmatrix}, \tag{11}$$

in terms of the reflection and transmission amplitudes of lead modes, $r^{(\prime)}$ and $t^{(\prime)}$.

For periodically driven systems, the scattering matrix associated with a Floquet operator can be computed in a slightly different fashion [60–62]. On a square lattice of $L \times W$ sites, the Floquet operator (6) is an $LW \times LW$ matrix. Rather than attaching infinite leads, we introduce absorbing terminals at the two sides of the system, $n_x = 1$ and $n_x = L$. Defining a $2W \times LW$ projector onto these terminals,

$$P = \begin{cases} 1 & \text{if } n_x \in \{1, L\}, \\ 0 & \text{otherwise,} \end{cases} \tag{12}$$

we can express the quasienergy-dependent Floquet scattering matrix through the formula

$$S(\varepsilon) = P\left[1 - e^{i\varepsilon}\mathcal{F}(1 - P^T P)\right]^{-1} e^{i\varepsilon}\mathcal{F}P^T, \tag{13}$$

where the superscript T denotes transposition. The expression (13) can be understood by expanding the inverse matrix in a geometric series, in which each subsequent term describes time evolution over an additional period. Time evolution stops after the state reaches the absorbing terminals, P, and continues otherwise, $1 - P^T P$ [51]. The absorbing terminals only act stroboscopically, at the beginning and end of each time period, such that Eq. (13) describes a simplified, fictitious scattering

problem. Nevertheless, the unitarity of the Floquet operator $\mathcal{F}$ implies that the scattering matrix is also unitary, $S(\varepsilon)S^\dagger(\varepsilon) = 1$, which can be verified though a direct calculation.

In this setup, the Floquet scattering matrix takes the form of Eq. (11), enabling us to compute the transmission from one side of the system to the other, $G = \text{Tr}\, t^\dagger t$. At $\varepsilon = \pi$, the presence of one pair of counterpropagating edge states leads to a quantized transmission $G = 2$, since there is one right- and one left-mover on each edge.

First we identify the constraints imposed by the chiral symmetry on S. Toward that end, we consider a system with an odd number of sites in the y direction (W odd), and we apply twisted boundary conditions, as $|n_x, W\rangle = e^{i\phi}|n_x, 0\rangle$. The Floquet operator, and therefore also the scattering matrix, now become functions of the twist angle ϕ, which plays the same role as momentum in the chiral symmetry constraint of Eq. (9). Plugging this constraint into the Floquet scattering matrix definition (13) leads to a relation

$$\Gamma_S S(\varepsilon, \phi)\Gamma_S = S^\dagger(-\varepsilon, \phi - \pi), \tag{14}$$

where Γ_S is a $2W \times 2W$ matrix defined by $\Gamma_S = P\Gamma_\mathcal{F}P^T$. In other words, Γ_S changes the sign of one sublattice in the absorbing terminals at $n_x = 1, L$.

The relation (14) is reminiscent of that found for chiral symmetric static systems [53], where at zero energy there exists a basis in which the scattering matrix is Hermitian. For the periodically driven system studied here, the π momentum shift induced on the Floquet level carries over in the scattering matrix description. Therefore, we introduce the chiral basis $\widetilde{S} = \Gamma_S S$, in which the reflection subblock obeys $\widetilde{r}(\phi) = \widetilde{r}^\dagger(\phi - \pi)$ at $\varepsilon = \pi$. This enables us to formulate a topological invariant by noting that for this quasienergy,

$$\det \widetilde{r}(\phi) = \det{}^* \widetilde{r}(\phi - \pi). \tag{15}$$

By Eq. (15), the complex phase of the determinant of $\widetilde{r}$ must change sign as the twist angle ϕ is advanced by π. Since the complex phase must be a continuous function of ϕ, only two scenarios are possible. In the interval $\phi \in [0, \pi]$ (half of the effective BZ), either the phase of $\det \widetilde{r}$ crosses 0 an odd number of times, or it crosses π an odd number of times, as shown in Fig. 4.

The odd number of 0-crossings or π-crossings in half of the BZ is a $\mathbb{Z}_2$ topological invariant, and it cannot change as long
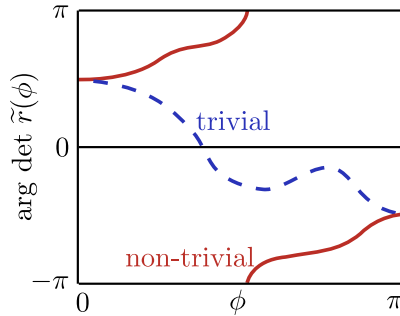
FIG. 4. Two possible ways in which the phase of det $\widetilde{r}$ can evolve as the twist angle is advanced from $\phi = 0$ to $\phi = \pi$. The solid and dashed lines indicate topologically different scenarios, since they cannot be deformed into each other as long as the bulk mobility gap remains open (det $\widetilde{r} \neq 0$). The presence of protected π-crossings signals a topologically nontrivial phase in our choice of gauge.

as there is a mobility gap in the bulk: det $\widetilde{r} \neq 0$. While the two scenarios are topologically different, which of them occurs is a matter of definition. To preserve the form of the chiral symmetry requirement (9), we have used an odd number of sites in the y direction, making $\widetilde{r}$ a matrix with odd dimensions. Therefore, depending on which of the two sublattices changes sign under the application of Γ_S, the determinant of $\widetilde{r}$ will also change sign, turning 0-crossings into π-crossings, and vice versa. For definiteness, we chose a gauge in which the chiral basis has det $\Gamma_S = -1$, and we identify π-crossings with a topologically nontrivial phase. Choosing the other sign would imply interchanging the labels of Fig. 4.

By numerically computing the reflection matrix as a function of twist angle, we have checked that this $\mathbb{Z}_2$ invariant correctly describes the topological phases of the model. Furthermore, the relation (15) still holds when disorder is added to the system, provided the latter does not break chiral symmetry. We therefore expect the edge state transmission to be robust upon the inclusion of random hopping strengths $J_{x,y}$. On the other hand, the system should fully localize if we add random on-site potentials, which violate the chiral symmetry requirement of Eqs. (8) and (15).

We confirm this numerically by including disorder in one of two ways. For random bond disorder, we substitute $J_{x,y} \rightarrow J_{x,y}(1 + \delta_J)$, with δ_J drawn independently for each bond from the uniform distribution $[-U,U]$, with U the strength of disorder. In the case of on-site disorder, we introduce a random, time-independent chemical potential term to the Hamiltonian (1), $\delta_\mu |n_x,n_y\rangle\langle n_x,n_y|$, where δ_μ is drawn independently for each lattice site from the same, uniform distribution. The transmission scaling results of Fig. 5 confirm our expectations. Bond disorder leads to an algebraic decay of the edge transmission, $G \sim 1/\sqrt{L}$, characteristic of two-dimensional statistical topological insulators [63]. The edge remains delocalized, being pinned to a one-dimensional critical point [18,64–67], and the phase of det $\widetilde{r}$ still shows protected π-crossings. In contrast, we find that on-site disorder leads to an exponential suppression of edge transmission, $G \sim \exp(-cL)$, $c = \text{const}$, signaling localization.

Before concluding this section, we analyze the top and bottom energy gaps appearing in Fig. 1. Away from $\varepsilon = 0,\pi$,
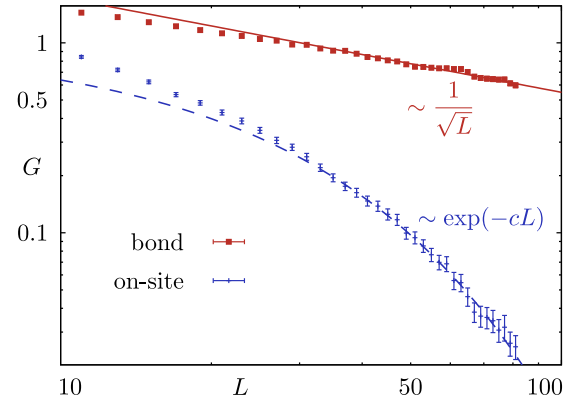

FIG. 5. Log-log plot of the edge transmission of model (6) at $\varepsilon = \pi$ as a function of system length L for bond (red) and on-site (blue) disorder, with $W = 40$, $\alpha = J_x = 2\pi/3$, and $J_y = 2\pi$. For on-site disorder we have used a disorder strength $U = 1.8$, while for bond disorder it was set to $U = 0.45$. In each case, 600–800 independent disorder realizations were averaged over. The solid and dashed lines show the expected algebraic and exponential decay of transmission, respectively.

the system does not obey chiral symmetry, and there is an imbalance in the number of left and right movers on an edge. Since these edge states manifest in the absence of any symmetries, the scattering matrix invariant originally developed to describe the Chern number of static systems [53,68] correctly captures the net chirality of the edge states. By applying twisted boundary conditions as before, we write the topological invariant as the winding number of det r,

$$C_{\text{SM}} = \frac{1}{2\pi i} \int_0^{2\pi} d\phi \, \frac{d}{d\phi} \log \det r(\phi). \qquad (16)$$

For the parameters in the left and right panels of Fig. 1, we find that the top gap has a scattering matrix Chern number $C_{\text{SM}} = +1$, while the bottom one has $C_{\text{SM}} = -1$. By repeating the calculation for the parameters of the middle panel, we find $C_{\text{SM}} = -2$ and $C_{\text{SM}} = +2$ for the top and bottom gaps, respectively.

As we have shown, scattering theory enables us to fully characterize the topological phases of the model (6). The counterpropagating modes appearing in the gap at $\varepsilon = \pi$ can be understood in terms of an invariant readily obtained by means of a symmetry analysis. Chiral modes present in other gaps are accounted for by the invariant (16), originally developed in the context of static Chern insulators. In the following section, we will further explore the connection between the scattering matrix invariants of static systems and the nontrivial phases of Floquet topological insulators.

III. PARTICLE-HOLE SYMMETRIC DRIVEN SYSTEM

One of the advantages of scattering theory in the study of periodically driven topological phases is that it allows for the study of both time-independent and Floquet topological insulators within the same unified framework. In this section, we use the scattering matrix formalism to reveal and characterize the rich structure of a model consisting of both strong and weak topological phases. As we will show, scattering matrix
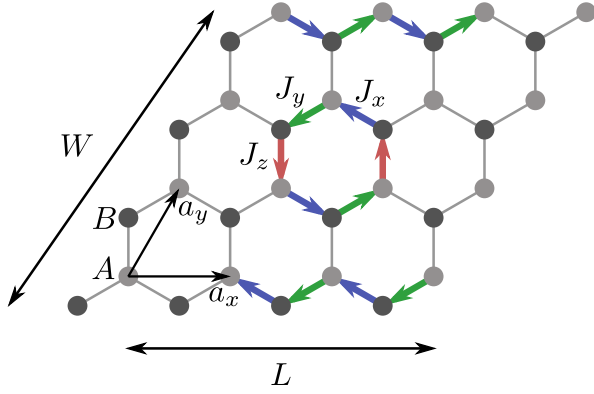
FIG. 6. Setup and driving protocol of Hamiltonian (18). We consider an $L \times W$ hexagonal lattice (sublattices A and B), with Bravais vectors a_x and a_y. When $J_u = 0$, only one of the hopping amplitudes $J_{x,y,z}$ (blue, green, and red, respectively) is turned on at any given time. For $J_s = \pi/2$, particles at any site in the bulk return to their original position after two driving periods, while those on the edges form chiral propagating modes, as shown by the arrows.

invariants of Floquet systems can take the same form as in their static counterparts, even when bulk Floquet bands fail to capture the nontrivial character of a phase.

We consider an example of particle-hole symmetric driven system, introduced in Ref. [45]. It describes spinless fermions on a hexagonal lattice in the presence of nearest-neighbor hopping. The unit cell consists of two sites belonging to the two sublattices, A and B, and the Bravais vectors of the lattice a_x and a_y are defined as in Fig. 6.

Setting the lattice constant to 1, the momentum-space tight-binding Hamiltonian has the form

$$H = \sum_{\mathbf{k}} (c_{A,\mathbf{k}}^{\dagger} c_{B,\mathbf{k}}^{\dagger}) \mathcal{H} \begin{pmatrix} c_{A,\mathbf{k}} \\ c_{B,\mathbf{k}} \end{pmatrix}, \qquad (17)$$

with

$$\mathcal{H} = [J_x \cos(k_y - k_x) + J_y \cos(k_y) + J_z]\sigma_x$$
$$- [J_x \sin(k_y - k_x) + J_y \sin(k_y)]\sigma_y. \qquad (18)$$

Here, $c_{A/B,\mathbf{k}}^{\dagger}, c_{A/B,\mathbf{k}}$ are fermionic creation and annihilation operators on the A and B sublattices, and $J_{x,y,z}$ are independent hopping amplitudes describing three different types of bonds, as shown in Fig. 6. The Pauli matrices σ_i appearing in $\mathcal{H}$ parametrize the sublattice degree of freedom.

In the absence of driving, the Hamiltonian (18) belongs to class BDI in the Altland-Zirnbauer classification [69]. It is characterized by time-reversal, particle-hole, as well as chiral symmetries, all of which square to $+1$. The corresponding operators are $\mathcal{T} = \mathcal{K}$, $\mathcal{P} = \sigma_z \mathcal{K}$, and $\mathcal{C} = \sigma_z$, with $\mathcal{K}$ complex conjugation, such that

$$\mathcal{H}(\mathbf{k}) = \mathcal{H}^*(-\mathbf{k}),$$
$$\sigma_z \mathcal{H}(\mathbf{k})\sigma_z = -\mathcal{H}^*(-\mathbf{k}), \qquad (19)$$
$$\sigma_z \mathcal{H}(\mathbf{k})\sigma_z = -\mathcal{H}(\mathbf{k}).$$

We choose a driving protocol that involves the cyclic modulations of the hopping amplitudes J_i [45]. Each of the three hoppings contains a uniform term J_u that is independent

of time τ, as well as a term J_s that is periodically varied in a stroboscopic manner. The three-step driving protocol reads as follows:

(i) $J_x = J_s + J_u, J_{y,z} = J_u$ for $nT < \tau \leqslant nT + T/3$,

(ii) $J_y = J_s + J_u, J_{z,x} = J_u$ for $nT + T/3 < \tau \leqslant nT + 2T/3$, and

(iii) $J_z = J_s + J_u, J_{x,y} = J_u$ for $nT + 2T/3 < \tau \leqslant nT + T$, with T the driving period.

In the following, we set $T = 3$ and $\hbar = 1$ expressing the Floquet operator as the product

$$\mathcal{F} = \exp(-i\mathcal{H}_3) \exp(-i\mathcal{H}_2) \exp(-i\mathcal{H}_1), \qquad (20)$$

where $\mathcal{H}_i$ are the Hamiltonians during the three steps of the driving protocol shown above. Even though at every instance of time the Hamiltonian (18) is time-reversal symmetric, the sequence in which the x-, y-, and z-type hoppings are modulated implies that the Floquet operator (20) has broken time-reversal symmetry.

In the simplest case, we set $J_u = 0$, such that during each of the three steps of the driving protocol only one of the $J_{x,y,z}$ hoppings is nonzero. When additionally $J_s = \pi/2$, a particle is transferred with unit probability between neighboring sites. Therefore, particles in the bulk fully encircle one hexagonal plaquette in two driving periods, leading to the formation of dispersionless (flat) bulk bands. In the presence of a boundary, the same driving protocol leads to the formation of a chiral propagating mode on the edge of the lattice, as shown in Fig. 6. We recover the dispersionless bulk bands as well as the chiral edge modes in the quasienergy band structure of the system [see Fig. 7(a)].

The emergence of the flat bulk bands attracts significant attention in its own right, in the context of possible realizations of exotic many-body phases in such systems [70–73]. In the case of a nontrivial topology of the flat band, reflected in the nonzero band Chern number, chiral edge states can emerge at the boundary of a finite system as a result of bulk-boundary correspondence.
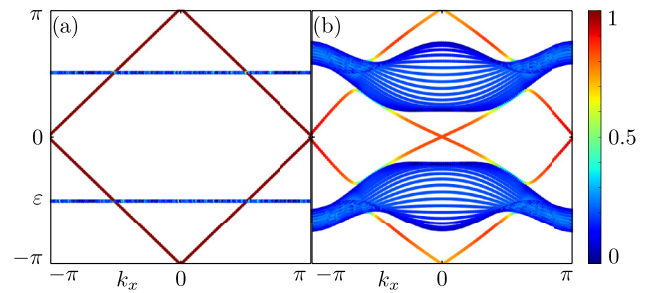

FIG. 7. Band structures of the model (18) at $J_s = \pi/2$ in a strip geometry (infinite along a_x, $W = 20$). In panel (a), $J_u = 0$ and there are two flat bulk bands at quasienergies $\varepsilon = \pm\pi/2$ as well as one chiral edge mode present at all quasienergies. In panel (b) we set $J_u = 0.25$, such that there is one chiral mode at $\varepsilon = \pi$ and a pair of counterpropagating modes at $\varepsilon = 0$. The strong and weak invariants at $\varepsilon = \pi$ read $(C_{\text{SM}}, \nu_{x,\pi}, \nu_{y,\pi}) = (-1, 1, 1)$ in both panels. At $\varepsilon = 0$, the system in panel (a) is in a $(-1, -1, -1)$ phase, while panel (b) has $(0, -1, -1)$. The color scale denotes the eigenstate intensity on the first and last 10% of lattice sites.

Interestingly, here for $J_u = 0$ and $J_s = \pi/2$ the bulk Floquet operator, $\mathcal{F} = i[\cos(k_x)\sigma_x + \sin(k_x)\sigma_y]$, is independent of k_y, meaning that both of the flat bands have zero Chern number, and all the bulk states are trivially localized. The topological protection of the edge states can nevertheless be deduced from the topological invariant formulated in Ref. [33], which takes into account the full time evolution of the Hamiltonian (18) throughout the driving cycle.

In the following, we show that in addition to reproducing this invariant, scattering theory can also reveal a much richer topological structure. Toward that end, we consider finite systems of size $L \times W$ (see Fig. 6), where L denotes the number of vertical bonds in the a_x direction and W is the number of zigzag chains in the a_y direction. The scattering matrix associated with the Floquet operator is obtained by introducing absorbing terminals on the first and last zigzag chain.

We repeat the analysis of Sec. II, finding that the presence of a chiral edge mode leads to a quantized transmission $G = 1$. As before, we apply twisted boundary conditions (twist angle ϕ) in the a_x direction, and we express the strong topological invariant as the winding number of $\det r$; see Eq. (16). Remarkably, the scattering matrix invariant originally developed to compute the Chern number of static systems correctly describes this phase, even though all bulk bands are trivial. We find that the scattering matrix Chern number equals $C_{\mathrm{SM}} = -1$ for all quasienergies ε in the bulk gaps of Fig. 7(a).

Beyond the topological classification in terms of the strong invariant, the Hamiltonian (18) shows a richer structure due to the presence of particle-hole symmetry. The cyclic nature of the driving protocol leads to a Floquet operator (20), which breaks time-reversal symmetry but shows particle-hole symmetry (PHS) of the form

$$\mathcal{F}(\mathbf{k}) = \sigma_z \mathcal{F}^*(-\mathbf{k})\sigma_z. \tag{21}$$

As such, for every eigenstate at quasienergy ε and momentum $\mathbf{k}$ there must be a state at $-\varepsilon$ and $-\mathbf{k}$. A chiral edge mode present at $\varepsilon = 0, \pm\pi$ must therefore exist at points where $\mathbf{k} = -\mathbf{k}$. This is the case for the band structure shown in Fig. 7(a), where the edge state crosses $k_x = 0$ for $\varepsilon = \pi$ and $k_x = \pi$ for $\varepsilon = 0$. The two edge-mode configurations at $\varepsilon = 0$ and $\varepsilon = \pi$ cannot be continuously deformed into each other without breaking particle-hole symmetry or closing the bulk gap, signaling that the two phases are topologically distinct.

In other words, the parity of edge modes at momenta $k_x = 0, \pi$ appearing in Fig. 7(a) is topologically protected. In a static topological superconductor, this protection would be expressed in terms of a weak invariant [17,18,74,75]. Motivated by this fact, we analyze the gapped phases of the model (20) in terms of the scattering matrix invariants developed to classify weak topological superconductors.

To identify how the invariant emerges, we analyze the symmetries constraining the scattering matrix. Plugging the particle-hole symmetry constraint (21) into the scattering matrix expression (13) leads to a relation

$$S(\varepsilon) = \sigma_z S^*(-\varepsilon)\sigma_z, \tag{22}$$

where σ_z acts on the sublattice degree of freedom in the absorbing terminals. As a consequence of Eq. (22), at the particle-hole symmetric quasienergies $\varepsilon = 0, \pi$ there exists a basis in which the scattering matrix, and therefore also its

reflection subblock, is real. We choose the basis $\tilde{r} = UrU^\dagger$, with $U = \mathrm{diag}(1, i, 1, i, \ldots, 1, i)$ such that $\tilde{r} = \tilde{r}^*$, and we introduce $\mathbb{Z}_2$ weak-scattering matrix invariants counting the parity of edge modes at $k_x = 0$ and π,

$$\begin{aligned} \nu_{x,0} &= \mathrm{sgn}\det\tilde{r}(\phi = 0), \\ \nu_{x,\pi} &= \mathrm{sgn}\det\tilde{r}(\phi = \pi). \end{aligned} \tag{23}$$

Here, $\phi = 0, \pi$ corresponds to applying periodic or antiperiodic boundary conditions in the a_x direction, respectively. The weak invariants in the a_y direction, $\nu_{y,0/\pi}$, can be defined in a similar manner by introducing absorbing terminals at $a_x = 1, L$ and using (anti)periodic boundary conditions along a_y [76].

The topological numbers of Eqs. (16) and (23) have features similar to those defined for static systems. The strong $\mathbb{Z}$ index counts the net number of chiral modes, whereas the weak $\mathbb{Z}_2$ invariants determine the parity of modes crossing at momentum 0 or π. As such, the weak invariants are constrained by the parity of the strong index C_{SM} as $\nu_{i,0}\nu_{i,\pi} = (-1)^{C_{\mathrm{SM}}}$, with $i = x, y$ [77]. Characterizing a topological phase, therefore, requires specifying C_{SM}, $\nu_{x,\pi}$, as well as $\nu_{y,\pi}$, since their values can change independently [11]. In accordance with the terminology used in static weak topological superconductors, we label a phase where an odd number of edge modes cross momentum π as nontrivial [17,78].

For $J_u = 0$ and $J_s = \pi/2$ we find that in both directions $i = x, y$ we have $\nu_{i,0} = -1$ and $\nu_{i,\pi} = 1$ at $\varepsilon = \pi$, while their signs are reversed at $\varepsilon = 0$. Therefore, the $\varepsilon = 0$ phase of Fig. 7(a) is nontrivial in both a strong and a weak sense. Even though the strong invariant $C_{\mathrm{SM}} = -1$ remains unchanged, weak indices can distinguish between the two phases, such that an interface between the phase at $\varepsilon = 0$ and $\varepsilon = \pi$ would host a pair of counterpropagating edge modes [11]. A purely weak phase is obtained in Fig. 7(b), where turning on a small uniform hopping, $J_u = 0.25$, changes the strong invariant to $C_{\mathrm{SM}} = 0$ while keeping $\nu_{i,\pi} = -1$ at $\varepsilon = 0$.

As in time-independent topological superconductors, the weak invariants introduced above are protected by the combination of PHS and translational symmetry of the system. Breaking the latter, for instance by introducing a staggered modulation of hopping amplitudes, would fold the quasi-BZ of Fig. 7 in momentum, converting the nontrivial weak invariants at $\varepsilon = 0$ into trivial ones. Nevertheless, we find that weak invariants are robust to disorder as long as the latter preserves translational symmetry on average, and the $\varepsilon = 0$ phase in Fig. 7(b) can be thought of as the periodically driven analog of a statistical topological insulator once disorder is introduced [63]. In this phase, we verify that adding a random component to J_u, drawn independently for each bond from a uniform distribution, leads to an algebraically decaying edge transmission $G \sim 1/\sqrt{L}$. The counterpropagating edge states avoid localization due to a combination of particle-hole symmetry and average translational symmetry, effectively forming a Floquet Kitaev edge [18].

There are, however, important differences between the topological classification of time-independent superconductors and that of the model (20). First, in periodically driven systems there are two PHS quasienergies at which the weak invariants can be defined, namely $\varepsilon = 0$ and π, allowing for a

richer topological structure. Even though the weak invariants at $\varepsilon = 0, \pi$ are protected by the same set of symmetries, namely PHS and translation along either a_x or a_y, they can vary independently of each other. This is to be contrasted with the topological classification of static systems [3,4,11] in which different invariants always require different sets of protecting symmetries.

Another feature unique to weak topological Floquet systems can be traced back to the periodicity of quasienergy. In static systems, a weak phase may be destroyed by a dimerization-induced breaking of translational symmetry, leading to a doubling of the unit cell and a folding of the BZ in momentum. In periodically driven systems, there is an extra direction in which the BZ can be folded, i.e., that of quasienergy. Such a breaking of *time-translation* symmetry can be achieved by introducing a half-frequency component in the driving protocol, effectively doubling the driving period. This leads to a new phase at $\varepsilon = 0$, with invariants $(C_{\mathrm{SM}}, \nu_{x,\pi}, \nu_{y,\pi})$ obtained by the composition of indices in the original (prefolding) $\varepsilon = 0$ and $\varepsilon = \pi$ phases. While in our example the folded phase is obtained simply by the $\mathbb{Z}$ addition of the strong index and the $\mathbb{Z}_2$ addition of the weak ones, more complex composition rules may apply in a generic setting [77].

We show an example of time folding in Fig. 8, obtained using inequivalent hopping amplitudes $J_{x,y,z}$ in Eq. (18). Setting $J_s = \pi/2$ and the uniform components to $J_{u,x} = -0.05$ and $J_{u,y} = J_{u,z} = 0.5$, we obtain phases with indices $(0,-1,-1)$ at $\varepsilon = 0$ and $(0,-1,1)$ at $\varepsilon = \pi$. The folding is implemented by repeating the three-step driving protocol described above

twice, and altering the stroboscopic component of J_x during every second period, as $J_{s,x} = J_s + \delta J_s$, with $\delta J_s = 0.6$. This leads to a new gapped phase at $\varepsilon = 0$, with invariants $(0,1,-1)$, obtained by the composition of the original ones.

IV. CONCLUSION

In many static systems, topological properties are fixed during the fabrication process. Part of the active interest in Floquet systems comes from the possibility to tune these properties by altering the driving protocol. Nevertheless, the topological classification of periodically driven systems has remained largely unexplored.

We have shown that topological phases of periodically driven systems can be analyzed in a unified framework by using scattering theory. In some cases, both static and Floquet systems may be characterized by the same scattering matrix invariants due to the similar transport properties of their edge modes. This has enabled us to reveal a richer topological structure in a previously studied model (Sec. III). We wrote down expressions for both strong and weak topological invariants, showing that they correctly describe the nontrivial phases even when all bulk bands are trivial.

When driven systems show weak phases for which no time-independent counterpart is known, as in Sec. II, scattering theory can be readily used to formulate novel invariants, based on the constraints imposed on the scattering matrix by the symmetries of the system. Since scattering matrix invariants are naturally tailored to the study of disordered systems, we were able to use their expressions to deduce the conditions under which the weak phase survives disorder.

Finally, we have shown that breaking translational symmetry in time can be used to alter the topological invariants of a phase. This novel feature is unique to Floquet topological insulators and allows a greater level of control in the design and manipulation of topological phases. Using the model of Sec. III, we have demonstrated this idea and altered the topological invariants of a weak phase by doubling the driving period.

We emphasize that, even though we have focused on two specific models, our scattering matrix approach to Floquet systems is completely general. For instance, it can also be applied to time reversal invariant Floquet topological insulators or higher-dimensional systems, as was the case for the scattering matrix invariants of static systems [53]. Our method is numerical in nature and requires systems large enough to avoid finite-size effects and show a well-defined bulk mobility gap. However, given a system size, Floquet scattering matrix invariants are more efficient to compute than those based on wave functions. No knowledge of Floquet eigenstates or time integration is required, and the biggest computational cost comes from inverting the time-evolution operator in Eq. (13).

We hope our work will pave the way toward a full classification of topological phases in periodically driven systems, which would parallel that of time-independent Hamiltonians. Additionally, our work will prove useful in determining the robustness to disorder of nontrivial phases, an essential ingredient for their experimental realization.
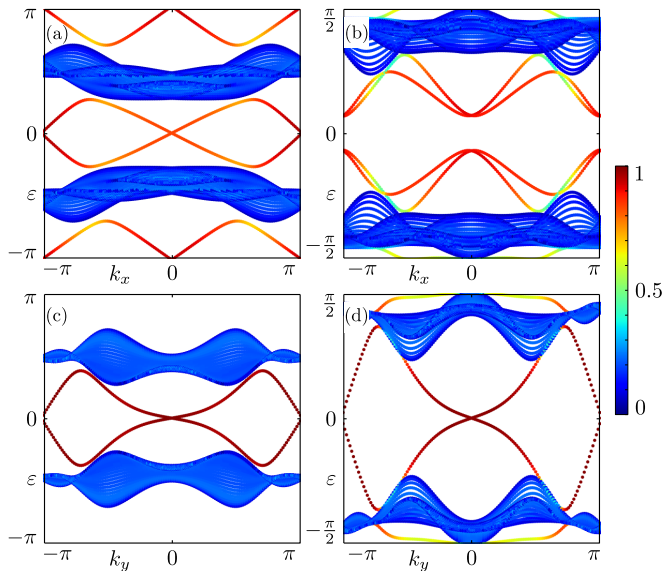

FIG. 8. Band structure of the model (18) in an infinite strip geometry with boundaries along the a_x (top, $W = 30$) and a_y (bottom, $L = 30$) directions. We use $J_s = \pi/2$ and inequivalent uniform components of the hopping amplitudes, $J_{u,x} = -0.05$, $J_{u,y} = J_{u,z} = 0.5$. In the right panels, the BZ is folded in quasienergy by changing the stroboscopic part of J_x to $J_{s,x} = \pi/2 + 0.6$ on every second period. The invariants of the prefolding phases (left panels), $(C_{\mathrm{SM}}, \nu_{x,\pi}, \nu_{y,\pi}) = (0,-1,-1)$ at $\varepsilon = 0$ and $(0,-1,1)$ at $\varepsilon = \pi$, combine to form a new gapped phase with $(0,1,-1)$ at $\varepsilon = 0$. The color scale denotes the eigenstate intensity on the first and last 10% of the lattice sites.

ACKNOWLEDGMENTS

[1] M. Z. Hasan and C. L. Kane, Rev. Mod. Phys. **82**, 3045 (2010).

[2] X.-L. Qi and S.-C. Zhang, Rev. Mod. Phys. **83**, 1057 (2011).

[3] A. Y. Kitaev, *Advances in Theoretical Physics*, edited by V. Lebedev and M. Feigel'man, AIP Conf. Proc. No. 1134 (AIP, New York, 2009), p. 22.

[4] A. P. Schnyder, S. Ryu, A. Furusaki, and A. W. W. Ludwig, *Advances in Theoretical Physics*, edited by V. Lebedev and M. Feigel'man, AIP Conf. Proc. No. 1134 (AIP, New York, 2009), p. 10.

[5] R.-J. Slager, A. Mesaros, V. Juričić, and J. Zaanen, Nat. Phys. **9**, 98 (2012).

[6] P. Jadaun, D. Xiao, Q. Niu, and S. K. Banerjee, Phys. Rev. B **88**, 085110 (2013).

[7] C.-K. Chiu, H. Yao, and S. Ryu, Phys. Rev. B **88**, 075142 (2013).

[8] F. Zhang, C. L. Kane, and E. J. Mele, Phys. Rev. Lett. **111**, 056403 (2013).

[9] W. A. Benalcazar, J. C. Y. Teo, and T. L. Hughes, Phys. Rev. B **89**, 224503 (2014).

[10] T. Morimoto and A. Furusaki, Phys. Rev. B **88**, 125129 (2013).

[11] M. Diez, D. I. Pikulin, I. C. Fulga, and J. Tworzydło, New J. Phys. **17**, 043014 (2015).

[12] J. E. Moore and L. Balents, Phys. Rev. B **75**, 121306(R) (2007).

[13] R. Roy, Phys. Rev. B **79**, 195322 (2009).

[14] L. Fu, C. L. Kane, and E. J. Mele, Phys. Rev. Lett. **98**, 106803 (2007).

[15] L. Fu, Phys. Rev. Lett. **106**, 106802 (2011).

[16] T. H. Hsieh, H. Lin, J. Liu, W. Duan, A. Bansi, and L. Fu, Nat. Commun. **3**, 982 (2012).

[17] I. Seroussi, E. Berg, and Y. Oreg, Phys. Rev. B **89**, 104523 (2014).

[18] M. Diez, I. C. Fulga, D. I. Pikulin, J. Tworzydło, and C. W. J. Beenakker, New J. Phys. **16**, 063049 (2014).

[19] Y. Tanaka, Z. Ren, T. Sato, K. Nakayama, S. Souma, T. Takahashi, K. Segawa, and Y. Ando, Nat. Phys. **8**, 800 (2012).

[20] P. Dziawa, B. J. Kowalski, K. Dybko, R. Buczko, A. Szczerbakow, M. Szot, E. Łusakowska, T. Balasubramanian, B. M. Wojek, M. H. Berntsen, O. Tjernberg, and T. Story, Nature Mater. **11**, 1023 (2012).

[21] S.-Y. Xu, C. Liu, N. Alidoust, M. Neupane, D. Qian, I. Belopolski, J. Denlinger, Y. Wang, H. Lin, L. Wray, G. Landolt, B. Slomski, J. Dil, A. Marcinkova, E. Morosan, Q. Gibson, R. Sankar, F. Chou, R. Cava, A. Bansil, and M. Hasan, Nat. Commun. **3**, 1192 (2012).

[22] C. Pauly, B. Rasche, K. Koepernik, M. Liebmann, M. Pratzer, M. Richter, J. Kellner, M. Eschbach, B. Kaufmann, L. Plucinski *et al.*, Nat. Phys. **11**, 338 (2015).

[23] J. Cayssol, B. Dóra, F. Simon, and R. Moessner, Phys. Status Solidi RRL **7**, 101 (2013).

[24] M. Bukov, L. DAlessio, and A. Polkovnikov, Adv. Phys. **64**, 139 (2015).

[25] N. Goldman and J. Dalibard, Phys. Rev. X **4**, 031027 (2014).

[26] N. H. Lindner, G. Refael, and V. Galitski, Nat. Phys. **7**, 490 (2011).

[27] Y. H. Wang, H. Steinberg, P. Jarillo-Herrero, and N. Gedik, Science **342**, 453 (2013).

[28] L. Jiang, T. Kitagawa, J. Alicea, A. R. Akhmerov, D. Pekker, G. Refael, J. I. Cirac, E. Demler, M. D. Lukin, and P. Zoller, Phys. Rev. Lett. **106**, 220402 (2011).

[29] A. Kundu and B. Seradjeh, Phys. Rev. Lett. **111**, 136402 (2013).

[30] A. A. Reynoso and D. Frustaglia, Phys. Rev. B **87**, 115420 (2013).

[31] M. Thakurathi, A. A. Patel, D. Sen, and A. Dutta, Phys. Rev. B **88**, 155133 (2013).

[32] M. C. Rechtsman, J. M. Zeuner, Y. Plotnik, Y. Lumer, D. Podolsky, F. Dreisow, S. Nolte, M. Segev, and A. Szameit, Nature (London) **496**, 196 (2013).

[33] M. S. Rudner, N. H. Lindner, E. Berg, and M. Levin, Phys. Rev. X **3**, 031005 (2013).

[34] G. Usaj, P. M. Perez-Piskunow, L. E. F. Foa Torres, and C. A. Balseiro, Phys. Rev. B **90**, 115423 (2014).

[35] G. Jotzu, M. Messer, R. Desbuquois, M. Lebrat, T. Uehlinger, D. Greif, and T. Esslinger, Nature (London) **515**, 237 (2014).

[36] W. Zheng and H. Zhai, Phys. Rev. A **89**, 061603 (2014).

[37] D. Carpentier, P. Delplace, M. Fruchart, and K. Gawędzki, Phys. Rev. Lett. **114**, 106806 (2015).

[38] M. Lababidi, I. I. Satija, and E. Zhao, Phys. Rev. Lett. **112**, 026805 (2014).

[39] L. Zhou, H. Wang, D. Y. Ho, and J. Gong, Eur. Phys. J. B **87**, 204 (2014).

[40] Z. Zhou, I. I. Satija, and E. Zhao, Phys. Rev. B **90**, 205108 (2014).

[41] A. Quelle, W. Beugeling, and C. Morais Smith, Solid State Commun. **215-216**, 27 (2015).

[42] D. Y. H. Ho and J. Gong, Phys. Rev. B **90**, 195419 (2014).

[43] A. G. Grushin, A. Gómez-León, and T. Neupert, Phys. Rev. Lett. **112**, 156801 (2014).

[44] D. Abanin, W. D. Roeck, and F. Huveneers, Phys. Rev. Lett. **115**, 256803 (2015).

[45] T. Kitagawa, E. Berg, M. Rudner, and E. Demler, Phys. Rev. B **82**, 235114 (2010).

[46] F. Nathan and M. S. Rudner, New J. Phys. **17**, 125014 (2015).

[47] M. Moskalets and M. Büttiker, Phys. Rev. B **66**, 205320 (2002).

[48] T. Kitagawa, T. Oka, A. Brataas, L. Fu, and E. Demler, Phys. Rev. B **84**, 235108 (2011).

[49] L. E. F. Foa Torres, P. M. Perez-Piskunow, C. A. Balseiro, and G. Usaj, Phys. Rev. Lett. **113**, 266801 (2014).

[50] P. M. Perez-Piskunow, G. Usaj, C. A. Balseiro, and L. E. F. Foa Torres, Phys. Rev. B **89**, 121401 (2014).

[51] A. Tajic, Ph.D. thesis, Leiden University, 2005.

[52] I. C. Fulga, F. Hassler, A. R. Akhmerov, and C. W. J. Beenakker, Phys. Rev. B **83**, 155429 (2011).

[53] I. C. Fulga, F. Hassler, and A. R. Akhmerov, Phys. Rev. B **85**, 165409 (2012).

[54] B. Tarasinski, J. K. Asbóth, and J. P. Dahlhaus, Phys. Rev. A **89**, 042327 (2014).

[55] D. R. Hofstadter, Phys. Rev. B **14**, 2239 (1976).

[56] J. K. Asbóth and H. Obuse, Phys. Rev. B **88**, 121406 (2013).

[57] J. K. Asbóth, B. Tarasinski, and P. Delplace, Phys. Rev. B **90**, 125143 (2014).

[58] C. W. Groth, M. Wimmer, A. R. Akhmerov, and X. Waintal, New J. Phys. **16**, 063065 (2014).

[59] See Supplemental Material at http://link.aps.org/supplemental/10.1103/PhysRevB.93.075405 for the source code of our numerical simulations.

[60] Y. V. Fyodorov and H. J. Sommers, JETP Lett. **72**, 422 (2000).

[61] A. Ossipov, T. Kottos, and T. Geisel, Phys. Rev. E **65**, 055209 (2002).

[62] J. P. Dahlhaus, J. M. Edge, J. Tworzydło, and C. W. J. Beenakker, Phys. Rev. B **84**, 115133 (2011).

[63] I. C. Fulga, B. van Heck, J. M. Edge, and A. R. Akhmerov, Phys. Rev. B **89**, 155424 (2014).

[64] P. W. Brouwer, A. Furusaki, I. A. Gruzberg, and C. Mudry, Phys. Rev. Lett. **85**, 1064 (2000).

[65] P. W. Brouwer, A. Furusaki, and C. Mudry, Phys. Rev. B **67**, 014530 (2003).

[66] O. Motrunich, K. Damle, and D. A. Huse, Phys. Rev. B **63**, 224204 (2001).

[67] I. A. Gruzberg, N. Read, and S. Vishveshwara, Phys. Rev. B **71**, 245124 (2005).

[68] G. Bräunlich, G. M. Graf, and G. Ortelli, Commun. Math. Phys. **295**, 243 (2009).

[69] A. Altland and M. R. Zirnbauer, Phys. Rev. B **55**, 1142 (1997).

[70] E. J. Bergholtz and Z. Liu, Int. J. Mod. Phys. B **27**, 1330017 (2013).

[71] S. A. Parameswaran, R. Roy, and S. L. Sondhi, C. R. Phys. **14**, 816 (2013).

[72] O. Derzhko, J. Richter, and M. Maksymenko, Int. J. Mod. Phys. B **29**, 1530007 (2015).

[73] M. Maksymenko, R. Moessner, and K. Shtengel, Phys. Rev. E **91**, 062103 (2015).

[74] D. Asahi and N. Nagaosa, Phys. Rev. B **86**, 100504(R) (2012).

[75] A. Bühler, N. Lang, C. V. Kraus, G. Möller, S. D. Huber, and H. P. Büchler, Nature Commun. **5**, 4504 (2014).

[76] As in static systems, computing the weak invariant requires an $L \times W$ lattice that extends over an odd number of both A and B sites. This avoids opening a minigap in the edge state spectrum. We use an odd L to compute ν_x, and an odd W for ν_y.

[77] Y. Ran, arXiv:1006.5454.

[78] Note that although the sign of det r is topologically protected, choosing the value $+1$ to represent a trivial system requires a specific basis choice for the scattering matrix, as in static systems.